Journal of Power Sources 245 (2014) 1035–1045

Contents lists available at SciVerse ScienceDirect

Journal of Power Sources

journal homepage: www.elsevier.com/locate/jpowsour

Study of the effect of temperature on Pt dissolution in polymer electrolyte membrane fuel cells via accelerated stress tests

S.R. Dhanushkodi [a,b], S. Kundu [b], M.W. Fowler [a,*], M.D. Pritzker [a]

[a] Department of Chemical Engineering, University of Waterloo, Waterloo, Ontario, Canada N2G 3G1
[b] Automotive Fuel Cell Cooperation, 9000 Glenlyon Parkway, Burnaby, British Columbia, Canada V5J 5J8

HIGHLIGHTS

- Development of new accelerated stress testing protocols for catalyst layer degradation.
- Estimation of effective Pt surface area as function of temperature and cycles.
- Empirical correlation between EPSA loss and performance loss.
- Prediction of position of Pt band in MEA.

ARTICLE INFO

Article history:
Received 19 March 2013
Received in revised form
2 July 2013
Accepted 3 July 2013
Available online 12 July 2013

Keywords:
Accelerated stress testing
Fuel cell catalyst
Durability
Voltage loss analysis
Electrochemical surface area

ABSTRACT

Operation of polymer electrolyte membrane fuel cells (PEMFC) at higher cell temperatures accelerates Pt dissolution in the catalyst layer. In this study, a Pt dissolution accelerated stress testing protocol involving the application of a potentiostatic square-wave with 3 s at 0.6 V followed by 3 s at 1.0 V was developed to test fuel cell membrane electrode assemblies (MEAs). The use of this Pt dissolution protocol at three different temperatures (40 °C, 60 °C and 80 °C) was investigated for the same membrane electrode assembly composition. Impedance analysis of the membrane electrode assemblies showed an increase in polarization resistance during the course of the accelerated stress testing. Polarization analysis and electrochemical active surface area (ECSA) loss measurements revealed evidence of increased cathode catalyst layer (CCL) degradation due to Pt dissolution and deposition in the membrane as the cell temperature was raised. Scanning electron microscope (SEM) images confirmed the formation of Pt bands in the membrane. A diagnostic expression was developed to estimate kinetic losses due to oxygen reduction using the effective platinum surface area (EPSA) estimated from cyclic voltammograms. The results indicated that performance degradation occurred mainly due to Pt loss.

1. Introduction

The U.S. Department of Energy lifetime targets for polymer electrolyte member fuel cells (PEMFCs) are 5000 h for automotive applications and 40,000 h for stationary applications [1]. Undoubtedly, highly durable and active electrocatalysts are needed to meet these targets. However, challenges exist regarding catalyst durability in order for fuel cells to become more competitive with internal combustion engines and conventional power sources. The state-of-the-art electrocatalyst layers in PEMFCs consist of nanosized platinum particles dispersed over carbon-based supports. Problems that affect their durability include platinum dissolution and carbon corrosion in the catalyst layer. Although great strides have been made in reducing Pt/C catalyst loading levels by more than 50-fold in the last few decades [1,2], catalyst cost is another drawback. Other alternatives are still not at a mature stage of development and cannot match the activities and stabilities that are possible with Pt-based catalysts. Thus, analysis of Pt dissolution mechanisms and cathode catalyst layer degradation is critically important. Consequently, over the last ten years, more attention has been placed on developing catalyst durability protocols such as accelerated stress tests (AST) to evaluate membrane electrode assemblies and ultimately to design and optimize catalyst layers and meet automotive sector requirements [3]. An important quantity commonly monitored over the course of accelerated stress tests is the loss of material in the cathode catalyst layer (CCL) that can have a significant impact on morphology and physicochemical processes. Other aspects that have received attention are phenomena affecting Pt/C catalyst stability such as sintering of Pt

* Corresponding author.
E-mail address: mfowler@uwaterloo.ca (M.W. Fowler).

0378-7753/$ – see front matter © 2013 Elsevier B.V. All rights reserved.
http://dx.doi.org/10.1016/j.jpowsour.2013.07.016

particles, dissolution of platinum and corrosion of the carbon support [4]. These processes are major causes of CCL degradation since the growth of Pt particles and dissolution of Pt into the membrane phase both reduce the electrochemical active surface area and electrocatalyst capacity [5].

Different accelerated stress tests such as the application of square-wave voltage cycles between 0.87 V and 1.2 V, in which the voltage is held for 30 s at each potential, have been used as tools to measure the stability of the catalysts [6]. Under such accelerated stress test conditions, Pt can undergo morphological changes due to both chemical and electrochemical reactions that bring about Pt migration, particle aggregation and dissolution especially at the cathode [7]. PEMFCs typically operate at ~80 °C, but also experience wide temperature fluctuations during normal drive cycles. Consequently, elevated temperature is an important factor influencing the state of Pt catalysts and accelerating electrode degradation [8]. Other mechanisms such as ionomer/membrane degradation and carbon corrosion are also responsible for the degradation of the membrane electrode assemblies [6]. To study these phenomena, potential cycling experiments in which parameters such as the upper and lower voltages, voltage waveform (square-wave, triangular wave or sinusoidal) and flow rate of input gases have been conducted [9,10].

Catalyst particle growth or platinum transfer into the membrane has been shown to depend on temperature, sweep potential and duration of the accelerated stress testing [3,7]. Platinum dissolution during operation of fuel cell stacks is considered to occur either when the load or voltage is varying or when it is at a constant high value typical of "idling" conditions [11]. Subjecting membrane electrode assemblies to fuel cell power train drive cycles can simulate both of these conditions. The extent of dissolution is governed by a complex interplay between electrochemical dissolution of metallic platinum, formation of platinum oxide and chemical dissolution of the oxide. Pt dissolution in acid media has been found to strongly increase with electrode potential in the region of 0.85–0.95 V *vs.* reversible hydrogen electrode (RHE) [12]. In another study, cycling the cell voltage between 1.2 V and 0.1 V was shown to degrade Pt catalysts [4]. The manner in which the potential is cycled has also been found to be important, with the application of slow triangular sweeps and square-waves causing the Pt dissolution rate to accelerate [9]. The dissolution rate also increases as the upper potential limit is raised from 0.8 V to 1.0 V during potential cycling of the cell. However, with further increase in the upper potential from 1.0 V to 1.2 V, carbon corrosion in addition to Pt dissolution [4] has been observed. The lower potential limit also affects catalyst degradation. A decrease in the lower potential limit from 0.6 V to 0.4 V leads to Pt re-deposition and reduction of Pt oxides [13]. Thus, application of cell voltages in the range of 0.6–1.0 V should be appropriate for assessing Pt dissolution from catalyst layer. As would be expected, Pt dissolution has also been shown to depend strongly on temperature and humidity [14,15]. The placement or deposition of the platinum in the catalyst layer is an important factor for achieving higher durability and performance by any membrane electrode assembly. Usually, the arrangement of Pt atoms depends on size of the Pt particle and its location on the support surface.

The hydrogen desorption peak in cyclic voltammograms (CV) obtained when H_2 is introduced on the anodic side and N_2 on the cathodic gives a measure of the surface area of Pt sites available for electrochemical reactions. Only those Pt atoms that are connected with the ionomer as well as the catalyst support serve as active reactive sites for fuel cell electrochemical reactions. The surface area of the Pt atoms connected with the ionomer and support is known as the effective platinum surface area (EPSA). The EPSA of the catalyst layer is generally smaller than the total platinum (chemical) surface area, also known as the electrochemical active surface area (ECSA), due to poor utilization (U_{Pt}) of the catalyst. A loss in EPSA and poor utilization of catalyst can increase the overpotential required to accelerate the electrochemical reactions, especially oxygen reduction (ORR). A study of the correlation between the EPSA and overpotential is required to improve the catalyst design and durability.

However, in spite of recent research that has led to new findings, testing protocols and methods to characterize the degradation of membrane electrode assemblies are still not well refined. Furthermore, accelerated stress testing protocols that focus primarily on catalyst layer degradation due to Pt dissolution are not well established. This is an aspect of PEMFC technology that requires further improvement. To date, no detailed study has been conducted to examine the role of Pt dissolution on catalyst degradation at different temperatures. Consequently, the main objectives of this study are to develop an accelerated stress test for Pt dissolution and use it to analyze the impact of temperature on catalyst layer (CL) degradation. For the current study, an accelerated stress test involving square-wave cycles between 0.6 and 1.0 V with a dwell times of 3 s at each cell voltage has been chosen to accelerate Pt dissolution by both chemical and electrochemical pathways [4,15]. Other aims of the current study are to develop a relationship between the EPSA and performance loss with the intention of shedding light on the mechanisms for Pt dissolution and to investigate the possible formation and location of Pt bands within the membrane.

2. Experimental

2.1. Preparation of membrane electrode assemblies

Membrane electrode assemblies were assembled using Core Automotive Testing (CAT) cell hardware developed by AFCC (Burnaby, British Columbia) [16]. The membrane electrode assembly components such as gas diffusion media and frames for both the cathode and anode catalyst-coated membrane were cut using a swing beam cutting press. The catalyst-coated membrane and gas diffusion media of the cathode and anode were aligned precisely with the frames and bonded to make a membrane electrode assembly with active geometric area of 48.4 cm^2. Graphitic carbon-supported platinum (40 wt% platinum) layers with platinum loading of 0.4 mg cm^{-2} and 0.1 mg cm^{-2} were deposited at the cathode and anode sides of the catalyst-coated membrane, respectively. Once assembled, the cell hardware was connected to a Hydrogenics Green Light G50 fuel cell test bench for durability testing.

2.2. Cell conditioning

Each membrane electrode assembly was first tested to ensure no internal or external leaks would occur. The cell was then conditioned at 1.7 A cm^{-2} for 12 h and the other conditions listed in Table 1. A pressurized bladder was used to provide compression to maximize fuel cell performance and contact between the membrane electrode assemblies and the conducting flow-field plates. The optimal bladder pressure was determined based on the performance of the cell for each cell assembly. Generally, the bladder pressure was maintained between 60 and 80 psi.

2.3. Polarization curve

To measure the performance losses during accelerated stress testing, polarization curves were obtained at 60 °C under identical conditions (Table 1) at the beginning-of-life (BOL) and after 1000, 10,000 and 20,000 potential cycles of each accelerated stress test protocol. The current–voltage characteristics of the membrane

Table 1
Testing conditions for MEAs in this study.

Operating conditions	Temp (°C)	Cathode pressure (kPa)	Anode pressure (kPa)	Fuel flow rate (slpm)	Oxidant flow rate (slpm)	Relative humidity %
Conditioning	60	270	250	2 (H_2)	10 (Air)	100
MEA Characterization						
Steady state performance @ 0.1 and 1.7 A cm^{-2}	60	270	250	2 (H_2)	10 (Air)	100
I–V analysis	60	270	250	2 (H_2)	10 (Air)	100
EIS	60	270	250	2 (H_2)	10 (Air)	100
CV	60	100	100	0.203 (H_2)	0.644 (N_2)	100
Pt dissolution AST						
MEA#1 at 40 °C	40	270	250	2 (H_2)	10 (Air)	100
MEA#2 at 60 °C	60	270	250	2 (H_2)	10 (Air)	100
MEA# 3 at 80 °C	80	270	250	2 (H_2)	10 (Air)	100

electrode assemblies were measured periodically during the accelerated stress tests using an electronic load RBL 232 (TDI electronic devices) connected to a fuel cell test bench. These polarization curves were obtained at the operating conditions specified in Table 1 in the presence of pure hydrogen and air. The fuel cell was operated at 1.7 A cm^{-2} for 20 min to allow the fuel cell and test station to stabilize before the polarization curve was obtained. The polarization curve was obtained galvanostatically by varying the cell current density from 2.4 to 0 A cm^{-2} at intervals of 0.1 A cm^{-2} and measuring the resulting cell voltage. The membrane electrode assembly was held at each current density for 15 min to ensure steady state was reached except at open-circuit where the cell was maintained for only 1 min to avoid OCV-induced degradation. The cell voltage plotted on the *I–V* curves at each current density represents the average value obtained over the last minute of polarization although data were logged every 10 s. The maximum test current density was set based on either the maximum current limit of the instrument load box or the current density at which the cell voltage was less than a minimum set point of 0.1 V. The anode and the cathode gas line temperatures were set at 5 °C above the cell temperature in order to avoid water condensation in the inlet gas lines. The fuel used during the polarization curve measurements was ultra-high purity hydrogen (99.999% certified grade).

2.4. Electrochemical impedance spectroscopy (EIS)

To investigate the changes in polarization (R_p) and ohmic resistances (R_s) during durability testing, electrochemical impedance spectroscopy (EIS) spectra were obtained at 60 °C under identical conditions (Table 1) for beginning-of-life and after 10,000 and 20,000 potential cycles of each accelerated stress test protocol. A Solatron model 1260 impedance analyzer connected to a Solartron model 1287 potentiostat/galvanostat was used for these measurements with the cathode exposed to compressed air and anode exposed to ultra-high pure hydrogen. For these experiments, the electrochemical circuit was operated with the counter electrode connected to the reference electrode via a shunt. EIS data were obtained using the potentiostatic mode by applying an AC signal with a 5 mV-amplitude on a 0.85 V DC cell voltage beginning at a frequency of 10 kHz and decreasing down to 10 mHz. Z-plot and Z-view software were used to obtain and analyze the EIS data and to generate Nyquist and Bode plots. The effective ohmic and polarization resistances of the membrane electrode assemblies were determined by fitting the EIS spectra with a basic equivalent circuit model.

2.5. Cyclic voltammetry

To assess the changes in electrochemical surface area changes during membrane electrode assembly testing, cyclic voltammetry (CV) curves were obtained at 60 °C under identical conditions at the beginning-of-life and after 1000, 10,000 and 20,000 potential cycles of each accelerated stress test (Table 1). The voltammetry experiments were conducted with a PAR model 273 potentiostat/galvanostat in order to determine the electrochemically active surface area. Once again, the counter electrode was connected to the reference electrode via a shunt. During CV experiments, hydrogen was passed through the anode and the cell voltage was cycled between 0.05 and 1.2 V at a scan rate of 20 mV s^{-1}. The electrochemical active surface area was determined from the hydrogen desorption peak in the under-potential region of the steady state CV obtained with the cathode exposed to N_2 and the anode to H_2. During this analysis, the N_2 and H_2 pressures at the working and counter electrodes, respectively, were both controlled to remain constant since their levels have been found to affect the charge measured under the 'under-potential' hydrogen desorption peak which is used to give the area occupied by a monolayer of H atoms. As shown previously, a monolayer charge density of 210 μC cm^{-2} on a smooth Pt surface is obtained when both gases are held at 100 kPa [5]. Consequently, both the N_2 and H_2 pressures were maintained at 100 kPa during these experiments for the purpose of estimating the electrochemical active surface area. Prior to the CVs, the cathode was purged using N_2 for 20–30 min, causing the cell voltage to drop.

Core-view software was used to analyze the CV data to determine the electrochemical active surface area. The electrochemical active surface area of the Pt catalyst expressed in m^2 g_{Pt}^{-1} can be determined from the area under the hydrogen desorption region of the CV using the following expression [17]:

$$\mathrm{ECSA} = \frac{Q_D}{K L_W A_g} \quad (1)$$

where L_w is the cathode loading of the membrane electrode assembly (mg_{Pt} cm^{-2}), A_g is the geometric area of the electrode (cm^2) and Q_D is the integrated area (expressed in units of μC) under the hydrogen desorption region in the CV between 0.05 V and 0.4 V *vs.* RHE corrected for the double layer capacitance of the carbon support and Pt. As discussed above, K was taken to be 210 μC cm^{-2} [18]. A loading level L_w determined from the wt % Pt added to the carbon powder in the ink of 0.4 mg Pt cm^{-2} was used throughout this study.

2.6. Pt dissolution accelerated stress test

In this study, the membrane electrode assemblies were subjected to accelerated stress tests in which the cell voltage was cycled between 0.6 V and 1.0 V so that Pt dissolution was the dominant mode of degradation. The accelerated stress tests were conducted at 40, 60 and 80 °C to study the impact of temperature on Pt dissolution. In order to simulate real-life vehicle operating

conditions, voltage cycling was performed using H_2/air mode instead of H_2/N_2 mode. Higher performance losses in catalyst durability testing have been reported by cycling with square-wave voltage signals than with triangular waves [9]. Hence, the use of square-waves was adopted to induce Pt dissolution in this study. A dwell period of 3 s at each of the upper and lower limits was selected for the following reasons based on previous findings in the literature [9]. At such dwell times, losses in electrochemical active surface area and mass activity tend to be high, the change in surface coverage of PtO_x strongly affects performance loss and carbon losses due to Pt oxide layer formation are minimized when the cell is held at an upper potential of 1 V. This waveform was applied for a total of 20,000 cycles which was taken to be the end-of-life (EOL) state in this study. The relative humidity of the reactant streams was maintained at 100% to minimize degradation of other membrane electrode assembly components such as the membrane. This enabled Pt degradation to be more effectively isolated from the other modes. The other operating conditions used during the accelerated stress tests are given in Table 1.

2.7. Recovery

Voltage cycling may cause a build-up of platinum oxide on the cathode catalyst and thus reduce cell performance. The following recovery procedure was used to bring the cell back to its nominal state, at which point the membrane electrode assembly diagnostic measurements were made. After completion of a specified number of cycles during an accelerated stress test, the load bank was turned off and the cathode was purged with N_2 at a rate of 1 slpm for 20 min. This procedure helped to remove excess water present in the catalyst layer [19]. Then the flow of air to the cathode was resumed and the cell was conditioned according to the procedure described in Section 2.2 above for 2 h before measuring membrane electrode assembly performance indicators such as the *I–V* curves, EIS spectra and CVs.

2.8. Scanning electron microscopy

After the completion of the electrochemical experiments, a fresh membrane electrode assembly and a degraded membrane electrode assembly were cut along a plane normal to the component layers and cast in epoxy to expose their cross-sections. The cross-sections were examined using a Philips XL30 scanning electron microscope (SEM) with backscattering detection at 350× magnification and 15 kV. The thicknesses of the membrane and catalyst layer were measured from these cross-sectional images.

3. Results and discussion

3.1. Polarization curve

The EOL and BOL polarization curves measured during the accelerated stress tests conducted at 40, 60 and 80 °C are shown in Fig. 1. Although the accelerated stress tests were conducted at these different temperatures, the measurement of all the polarization curves were carried out at a standard temperature and pressure of 60 °C and 270/250 bar_g, respectively, to be able to make fair comparisons (Table 1). The performance degrades at all cell voltages during all three accelerated stress tests compared to the beginning-of-life performance. Comparison of the end-of-life curves with beginning-of-life demonstrates that significant degradation during the accelerated stress tests occurs in the low-current-density region between 0 and 0.2 A cm^{-2} at all three temperatures. The performance losses in the low current region where kinetic factors tend to be dominant likely arise due to changes in catalyst activity,

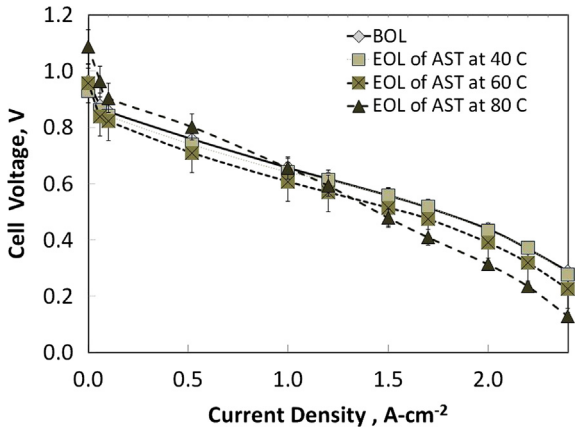

Fig. 1. Polarization curves of MEAs in BOL state and EOL states after being subjected to Pt dissolution ASTs at 40, 60 and 80 °C. Conditions during AST and polarization measurements are given in Table 1.

catalyst area and polarization resistance. At 80 °C, some additional degradation is observed at intermediate and higher currents. The open circuit voltage drops at a low rate of 0.08, 0.1 and 0.217 μV $cycle^{-1}$ at 40, 60 and 80 °C, respectively, during the course of the accelerated stress tests, suggesting that very little hydrogen crossover is occurring. Similar observations of low crossover were reported by Inaba et al. for membrane electrode assemblies cycled at 80 °C and 60 °C [20].

The decrease in cell performance is characterized in terms of the decrease in cell voltage measured at a current density of 1.7 A cm^{-2} after *N* cycles relative to that obtained in the BOL state at the same current density:

$$\text{Voltage loss} = E_{\text{BOL, 1.7 A cm}^{-2}} - E_{\text{N, 1.7 A cm}^{-2}} \quad (2)$$

The voltage losses of the membrane electrode assemblies in their EOL states after being subjected to accelerated stress tests at 40, 60 and 80 °C are approximately 30, 50 and 90 mV, respectively, reflecting that the polarization losses increase as the temperature is raised. These results suggest that only a relatively small loss in cell performance occurs at 40 °C, but that considerably more degradation is observed at 80 °C.

3.2. Changes in cell voltage and ECSA during accelerated stress tests

Fig. 2a shows the variation in the loss of cell potential with the number of cycles at the three temperatures at a current density of 0.1 A cm^{-2}, while Fig. 2b presents the corresponding curves for a current density of 1.7 A cm^{-2}. The plots indicate that the performance loss decays more rapidly as both temperature and current density rise. Voltage decay rates are determined using the following expression:

$$\text{Voltage decay rate} = \frac{E_{\text{BOL, 0.1 A cm}^{-2}} - E_{\text{N, 0.1 A cm}^{-2}}}{N} \quad (3)$$

Voltage loss rates of 0.96, 1.8 and 4.5 μV $cycle^{-1}$ measured at 0.1 A cm^{-2} are obtained at 40, 60 and 80 °C, respectively. At 1.7 A cm^{-2}, the measured potential decay rates are 1.75, 2.5 and 5 μV $cycle^{-1}$ at 40, 60 and 80 °C, respectively. In previous studies, higher cell potential loss rates of 30 and 20 μV $cycle^{-1}$ at 0.1 A cm^{-2} during square-wave potential cycling were reported [6,21]. However, the conditions during these studies differed considerably from those of the current study in many regards: cell temperature, cathode catalyst composition and design, method of material

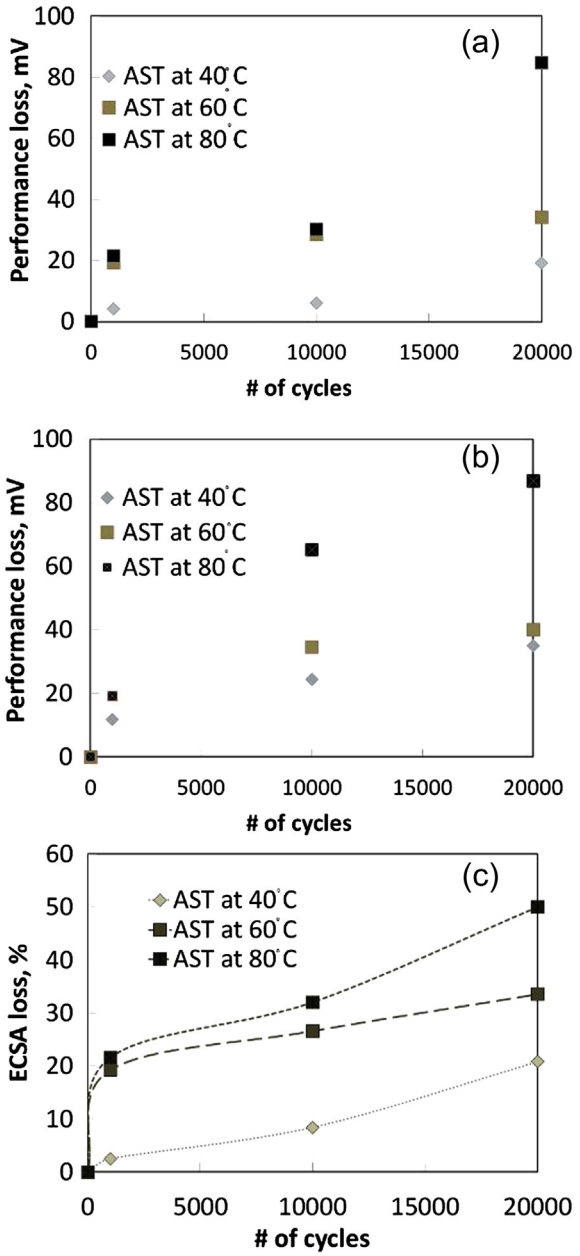

Fig. 2. Performance loss of MEAs measured after being subjected to Pt dissolution ASTs at 40, 60 and 80 °C. Performance loss obtained from polarization curves at (a) 0.1 A cm^{-2} and (b) 1.7 A cm^{-2}. Variation of % ECSA loss with number of cycles during the AST is shown in (c). Conditions during AST and polarization measurements are given in Table 1.

preparation, membrane electrode assembly hardware, upper and lower potentials during cycling and dwell time at the upper and lower potential limits. At 40 and 60 °C, the drop in cell potential at 0.1 A cm^{-2} is steep at the outset of cycling, but then levels off thereafter (Fig. 2a). On the other hand, the voltage measured during the accelerated stress test conducted at 80 °C exhibits higher degradation during the last 10,000 cycles compared to the first 10,000 cycles. Consistent with this trend is the observation (not shown here) that the voltage decay rate at this current measured between cycles is 3 times higher during the last 10,000 cycles than during the first 10,000 cycles when the MEA is degraded at 80 °C. When the performance loss at 1.7 A cm^{-2} is measured, the loss in cell voltage follows a similar trend at the three temperatures. The decay is largest over the first 1000 cycles and then slows down thereafter although the degradation is much larger at 80 °C than at the lower temperatures (Fig. 2b).

Six consecutive CVs between 0.6 and 1.2 V were conducted periodically during the accelerated stress tests at the three temperatures to determine the influence of potential cycling on the electrochemical active surface area. The ECSA for all the membrane electrode assemblies is calculated using Equation (1) on the basis of the last of the 6 CVs. The effect of cycle number on % loss of electrochemical active surface area at the three temperatures is shown in Fig. 2c. The electrochemical active surface areas of the three membrane electrode assemblies in their BOL state are found to be very close to each other, showing only a slight variation with a mean value of 80 ± 1.0 $m^2\ g^{-1}$. To account for this slight variation, the electrochemical active surface area data at each temperature are presented as the percentage loss from the BOL area of the respective membrane electrode assembly to normalize for the sample-to-sample differences. Overall, the loss in electrochemical active surface area increases as the temperature rises. At 40 °C, the electrochemical active surface area decreases from 80 to 63.4 $m^2\ g^{-1}$ (corresponding to a 21% loss) over the course of the accelerated stress testing until the end-of-life state is reached. This decrease is gradual with a slight increase in rate after 10,000 cycles are applied. The decrease in electrochemical active surface area at 60 °C from 81 $m^2\ g^{-1}$ in the BOL state to 54 $m^2\ g^{-1}$ in the EOL state corresponds to a 33% loss. However, this loss does not occur uniformly with time and is steep during the first 1000 cycles of the accelerated stress testing before leveling off and rising linearly and more slowly thereafter. The behavior observed at 80 °C is qualitatively similar to that at 60 °C, with the electrochemical active surface area dropping from 81 to 40 $m^2\ g^{-1}$ (50.6% loss) over the course of the accelerated stress testing.

3.3. Electrochemical impedance spectroscopy (EIS)

The Nyquist plots obtained from the EIS experiments during the Pt dissolution accelerated stress tests at the three temperatures are shown in Fig. 3a–c. Each spectrum exhibits a semi-circle with a high-frequency intercept equal to the ohmic resistance of the membrane and a low-frequency intercept equal to the sum of the ohmic resistance of the membrane and the charge transfer resistance of the catalyst layer [22]. In order to focus on the kinetics of the cathodic reaction, the impedance is measured at a low overpotential with pure hydrogen at the anode and high air flow rate at the cathode in order to minimize possible mass transport effects at the cathode and anode. Several trends are evident from the spectra. The membrane electrode assemblies in their BOL state generally exhibit lower impedance, particularly at lower frequencies, than those that have been subjected to accelerated stress tests at all temperatures. The diameter of the semi-circular arc in the Nyquist plots increases during the course of degradation at all three temperatures (Fig. 3). This is due primarily to a rise in the polarization resistance as the membrane electrode assemblies age from their BOL to EOL states. This effect is particularly strong at 80 °C, as shown in Fig. 3c.

The charge transfer (R_p) and ohmic (R_s) and resistances obtained from the fitting of equivalent circuit models to the EIS spectra are presented in Fig. 4a and b. During the accelerated stress test at 40 °C, R_p increases at a very low average rate of 1 μΩ-cm^2 $cycle^{-1}$ from 0.095 to 0.116 Ω-cm^2 (Fig. 4a). At an operating temperature of 60 °C, R_p increases at a faster average rate of 2 μΩ-cm^2 $cycle^{-1}$ from 0.101 to 0.137 Ω-cm^2. This trend continues at a temperature of 80 °C as the resistance increases from 0.110 to 0.161 Ω-cm^2 for an average rate of 2.5 μΩ-cm^2 $cycle^{-1}$. This increase is likely caused by the higher rate of Pt dissolution at 80 °C than at 40 °C, which leads to

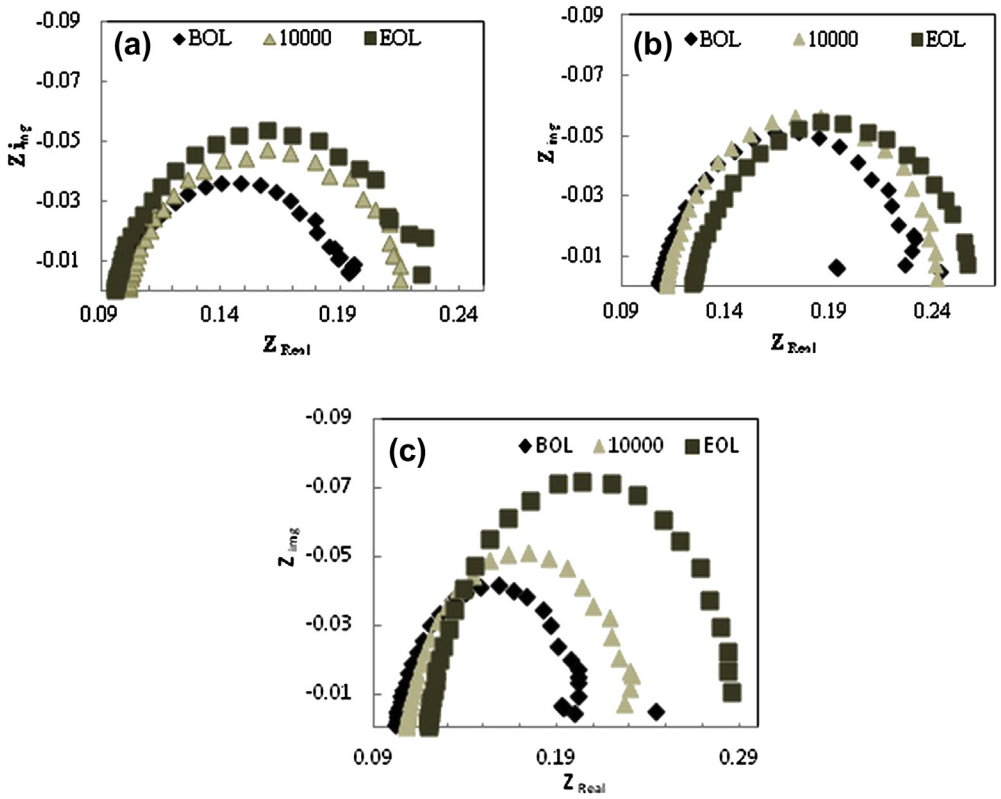

Fig. 3. Nyquist plots of MEAs obtained during the ASTs at (a) 40 °C, (b) 60 °C and (c) 80 °C. Conditions during AST and EIS measurements are given in Table 1.

significantly higher cell impedance in the EOL state. It should be noted that the R_p does not increase linearly throughout the accelerated stress testing. At all three temperatures, it increases at a much higher rate of approximately 6 μΩ-cm^2 cycle^{-1} during the first 1000 cycles than it does later during the testing. In fuel cells, R_s can be considered to be a combination of electronic and ionic resistances within the membrane and catalyst layer [22]. Since the humidity of both the cathode and anode of the cell is kept at 100% at all three temperatures, one would not expect significant changes in the initial R_s in the three cases, as confirmed in Fig. 4b. Furthermore, R_s remains virtually unchanged as the membrane electrode assemblies age at 40 °C and 60 °C. At 80 °C, on the other hand, R_s remains constant up to approximately 10,000 cycles, whereupon it begins to rise at a rate of ∼2 μΩ-cm^2 cycle^{-1} and reaches 0.129 Ω-cm^2 by the end of the test. This behavior suggests that the carbon support and/or the recast ionomer at the electrolyte–catalyst interface may have begun to degrade at this higher temperature [11]. This could cause the ionic conductivity of the ionomer in the catalyst layer and membrane to decrease enough for R_s to rise during the final 10,000 cycles of the accelerated stress test. This conclusion is supported by the polarization curve at 80 °C which showed some additional degradation in cell voltage at intermediate currents where ohmic effects become important (Fig. 1). This effect is not observed at the lower temperatures.

Overall, these results indicate that temperature has a stronger effect on the chemical and morphological stability of the catalyst layer and the Pt dissolution rate at 80 °C than at 40 or 60 °C. Thus, one must exercise caution in extrapolating the behavior observed at lower temperatures to accurately predict the behavior at 80 °C which is the typical operating temperature of PEMFCs.

Plots of R_s and R_p against electrochemical active surface area loss for all three accelerated stress tests are shown in Fig. 4c. A near linear dependence of R_p on electrochemical active surface area loss is observed at all three temperatures. Since electrochemical active surface area gives a measure of the amount of electrocatalyst that is electrochemically accessible during the accelerated stress testing, this suggests that the loss of active electrocatalyst contributes significantly to the loss in cell voltage observed from the polarization experiments (Figs. 1, 2a and b). The values of R_s shown in Fig. 4c reveal that temperature and the extent of degradation have very little effect on the correlation. This is important since it validates the experimental procedure adopted during this study. Recall that fuel cell performance during the accelerated stress testing is always characterized at 60 °C regardless of the temperature during these accelerated stress tests so that temperature effects during the characterization of cell performance would not be confounded with temperature effects on Pt degradation during potential cycling. The results also validate the decision to operate the cell at 100% relative humidity during the tests at the three temperatures to ensure that the ohmic resistance would not change significantly.

3.4. Changes in the morphology of the membrane electrode assembly

SEM images of BOL and EOL membrane electrode assemblies after being subjected to accelerated stress tests at 40, 60 and 80 °C have been obtained to examine whether phenomena such as dissolution and redeposition of Pt in the membrane occurred. The images presented in Fig. 5a–d confirms that some Pt in the catalyst layer has dissolved and formed Pt bands at all three temperatures by the time that the end-of-life is reached. No Pt is detected elsewhere in the membrane other than in these bands. The formation of Pt bands has been widely reported in previous durability studies focusing on degradation of the Pt/C catalyst. The only apparent difference between the BOL MEA and the EOL MEA subjected to an accelerated stress test at 40 °C is the presence of a thin platinum

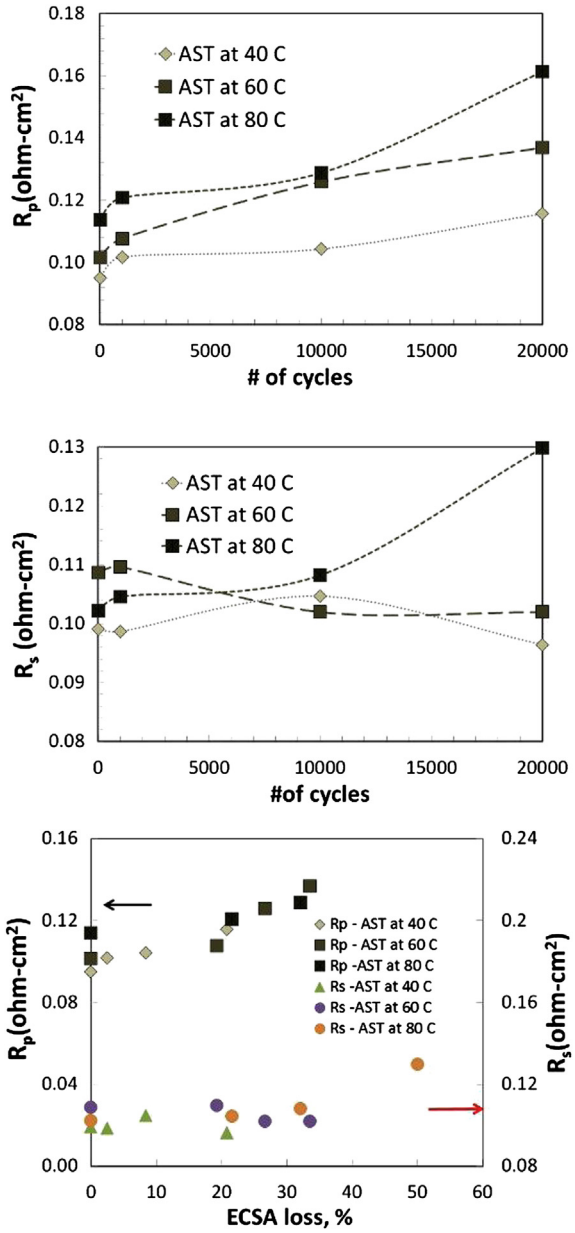

Fig. 4. Variation of the (a) R_p and (b) R_s with the number of cycles during ASTs at 40, 60 and 80 °C. Correlation of R_p and R_s to % ECSA loss during AST at 40, 60 and 80 °C is shown in (c). Conditions during ASTs and EIS measurements are given in Table 1.

band in the membrane near the CCL. The Pt bands in the images of the MEAs tested at 60 and 80 °C appear more intense than the one tested at 40 °C, similar to the trend reported by Bi and Fuller [23] and reflecting that more Pt has dissolved from the CCL and re-deposited in the membrane at the higher temperatures.

In previous studies, the following expression has been developed and/or used to predict the location of Pt bands [6,23,24]:

$$\frac{1}{x} = 1 + \frac{\alpha_{H_2/O_2}}{2}\frac{p_{H_2}}{p_{O_2}} \quad (4)$$

where p is the gas partial pressure and x is the dimensionless distance in the membrane. The location $x = 0$ corresponds to the cathode catalyst layer/membrane interface and $x = 1$ to the anode catalyst layer/membrane interface. α_{H_2/O_2} is the ionomer membrane selectivity defined as $D_{H_2}H_{H_2}/D_{O_2}H_{O_2}$ where D_{H_2} and D_{O_2} are the effective diffusivities of H_2 and O_2, respectively, and H_{H_2} and H_{O_2} are the Henry's Law constants for H_2 and O_2, respectively, in the membrane. Based on these calculations, a Pt band is predicted to form at 3.2 μm, 4.6 μm and 5.2 μm from the cathode for the three MEAs tested at 40, 60 and 80 °C, respectively. These are in excellent agreement with the band locations of 3.1, 4.8, and 5.1 μm estimated from the SEM images.

In view of these results, Pt band formation is considered to occur by a process consistent with the model that forms the basis for Equation (4). During the accelerated stress tests, some of the Pt within the cathode CL oxidizes and dissolves according to the reaction

$$Pt^0 \rightarrow Pt^{2+} + 2e^- \quad (5)$$

particularly when the cell voltage is at or near the upper limit of 1.0 V during a pulse cycle. Some of this Pt^{2+} re-precipitates elsewhere within the cathode CL and tends to coarsen the existing Pt particles, while the remainder diffuses into the membrane. At some point in the membrane, this Pt^{2+} comes into contact with H_2 crossing over from the anode and is chemically reduced back to Pt^0 by the reaction.

$$Pt^{2+} + H_2 \rightarrow Pt^0 + 2H^+ \quad (6)$$

Once Pt^0 has formed, it serves as catalyst for the overall reaction

$$2H_2 + O_2 \rightarrow 2H_2O \quad (7)$$

which occurs as a short-circuited galvanic cell comprised of the half-cell reactions

$$O_2 + 4H^+ + 4e^- \rightarrow 2H_2O \quad (8)$$

$$2H_2 \rightarrow 4H^+ + 4e^- \quad (9)$$

Since the gas fluxes entering the membrane are much greater than that of Pt^{2+}, Reaction (7) is the dominant process by which H_2 is consumed within the membrane. The potential of the Pt^0 particles is therefore given by the mixed potential at which the rate of consumption of electrons by the half-cell Reaction (8) is balanced by their rate of generation by Reaction (9). In the early stages of the potential cycling, the Pt^0 formed by Reaction (6) is located close to the cathode where O_2 is present at much higher levels than H_2. Due to this excess O_2, all of the H_2 that reaches the Pt^0 particles is consumed by Reaction (7). This also has the effect of driving the mixed potential of the Pt particles to ~1.0 V which is much too high for them to be stable. Consequently, any Pt particles previously formed are re-oxidized to Pt^{2+} and disappear, enabling the Pt^{2+} ions to diffuse closer to the anode. As the ions move toward the anode, this process of Pt deposition by Reaction (6) and re-dissolution is repeated again and again as long as the O_2 content in the membrane remains in excess over the H_2 content. Since the Pt^{2+} ions are moving in the direction of increasing H_2 content, a situation is eventually reached where the Pt particles formed by Reaction (6) are in a region in which the H_2 content begins to exceed that of O_2. This causes the mixed potential on the Pt particles to drop sharply to ~ 0–0.1 V which is now low enough for the particles to remain stable. Since a large excess of H_2 over Pt^{2+} exists at this location within the membrane, all of the Pt^{2+} is consumed by Reaction (6). As a result, no Pt^{2+} remains to move past this point and so this position marks the furthest advance of the ion. Thereafter, Reactions (6) and (7) proceed at a steady state. No further change in the position of the Pt band is observed although it can continue to thicken as more Pt^{2+} dissolves from the cathode, if time is allowed. This situation also ensures that all of the Pt deposition is

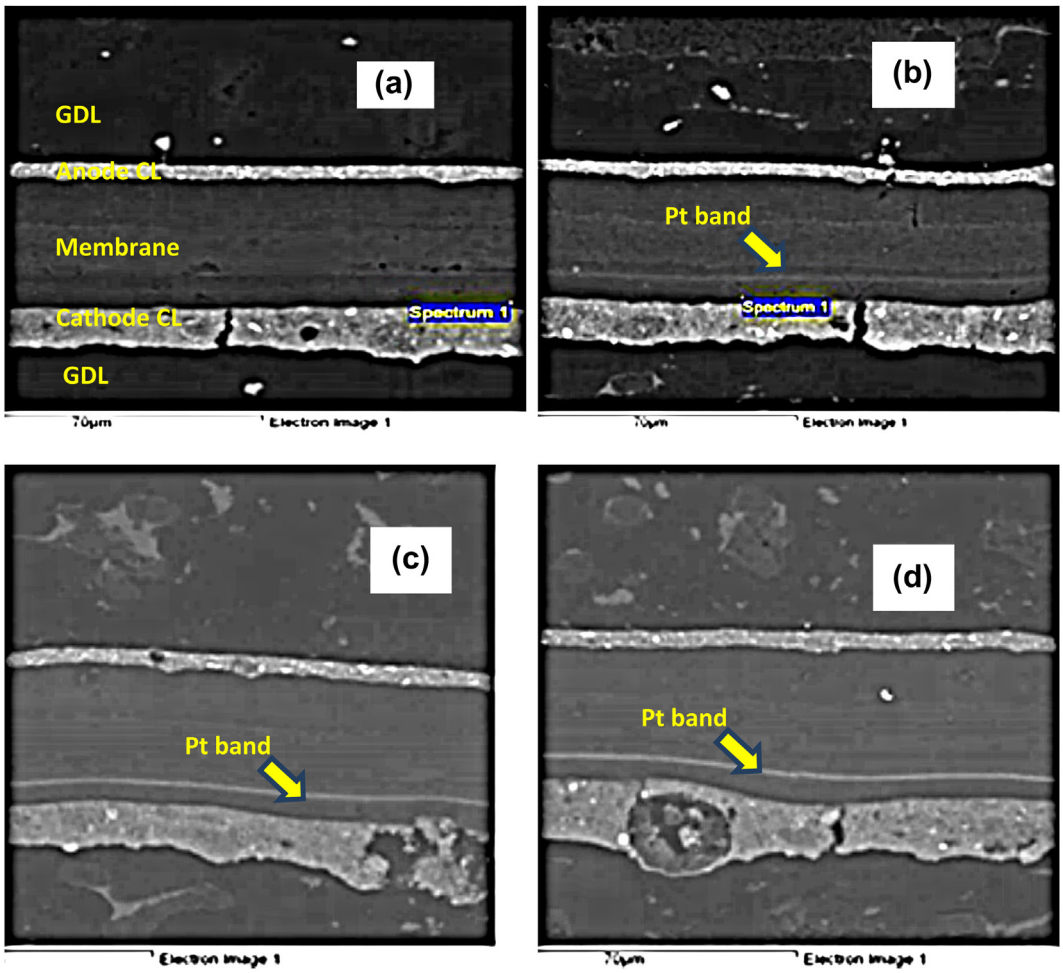

Fig. 5. SEM images of MEA samples in (a) BOL state and EOL states after ASTs at (b) 40 °C, (c) 60 °C and (d) 80 °C.

confined to a single location between the electrodes and leads to the appearance of a band.

The Pt band therefore forms in the narrow region where the mixed potential drops abruptly from ~1.0 V to ~0.1 V, which also corresponds to the location where H_2 and O_2 are simultaneously depleted. The molar fluxes of H_2 and O_2 across the membrane are governed by the stoichiometry of the dominant Reaction (7), i.e., $N_{H_2} = -2N_{O_2}$. This relationship between the fluxes and the condition of simultaneous depletion of H_2 and O_2 at the Pt particle surfaces uniquely define the Pt band location and ultimately lead to Equation (4).

The measurements and use of Equation (4) show that the location of the Pt band moves further from the cathode CL as the cell temperature is increased. This effect is explained by the fact that the rise in temperature increases the O_2 permeability $(i.e., D_{O_2}H_{O_2})$ relative to that of H_2 and so the point where O_2 becomes depleted moves away from the cathode.

3.5. Diagnostics of cell performance and effective platinum surface area loss

When the cell operates under kinetically controlled conditions, the degradation in its performance should be directly related to the loss in Pt catalyst surface area. In this section, we address this question directly by presenting a theoretical expression relating the kinetic overpotential at a given current density to the loss in the EPSA and applying it to experimental data. The computation of the EPSA requires that U_{Pt} and ECSA be known first. Once Q_D is determined from the CVs, ECSA is calculated using Equation (1). For the MEA used in this study, the ECSA in the BOL state is found to be 80 $m^2_{Pt}\ g^{-1}_{Pt}$, while U_{Pt} is taken to be 0.80 based on a previous study [25]. The EPSA of the BOL MEA is determined using Equation (A3) (see Appendix) to be 224 $cm^2_{(Pt)}\ cm^{-2}_{(geom)}$. A good measure of catalyst activity is the current density determined at a given overpotential. The effect of the EPSA loss is examined at a low current density near the start of the Tafel region where interferences from hydrogen crossover and mass transfer effects would be minimized [26]. Consequently, on the basis of the polarization curves, the performance loss is measured at 0.1 A cm^{-2} at the three temperatures. At this current density, overpotentials are in the range of 10–100 mV where kinetic effects dominate MEA performance.

The performance degradation expressed in terms of the drop in cell voltage obtained at 0.1 A cm^{-2} relative to that measured in the BOL state is plotted versus the % EPSA loss obtained after 1000, 10,000 and 20,000 cycles at 40, 60 and 80 °C in Fig. 6. Not surprisingly, a strong correlation between these two quantities is observed. After 20,000 cycles, the effective platinum surface area loss of 33% at 60 °C is higher than the 20% measured at 40 °C presumably due to the greater decrease in the Pt surface area at the higher temperature. The corresponding performance losses at 60 and 40 °C are 34 and 20 mV, respectively, at this current when end-of-life is reached. The effective platinum surface area and performance losses at 80 °C are even higher, reaching 50% and 84 mV, respectively, by the end of 20,000 cycles. The relationship

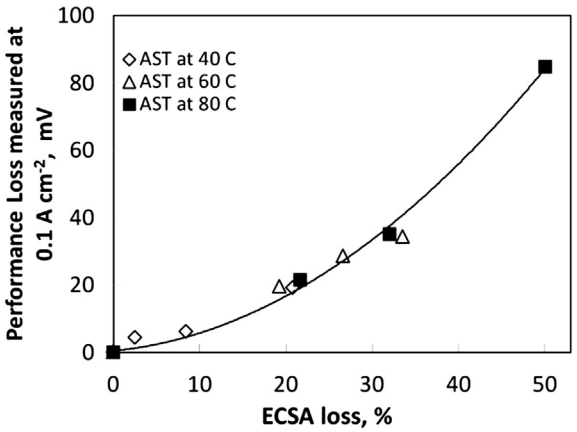

Fig. 6. Correlation between performance losses as measured from polarization at 0.1 A cm^{-2} and % ECSA loss during ASTs at 40, 60 and 80 °C.

between performance loss and % effective platinum surface area loss becomes less linear at 80 °C and, in fact, may have been qualitatively different than at the lower temperatures since it appears to accelerate as the cycling proceeds. Another factor contributing to the deviation from linearity could be the migration of dissolved platinum ions into the membrane during the accelerated stress test which has been shown to occur more readily at higher temperatures [8]. The SEM image shown in Fig. 5d confirms that Pt migration and band formation have occurred.

Despite these possible effects, perhaps the most striking feature of Fig. 6 is that the data lie along a single universal curve regardless of the temperature maintained during the accelerated stress tests. This observation supports the idea above that the degradation in performance should be directly related to the loss in Pt catalyst surface area when the cell operates under kinetically controlled conditions. Moreover, given that the cathodic reaction controls the kinetics under normal operating conditions, one would also expect the loss in EPSA to directly affect the activation overpotential associated with the oxygen reduction reaction (ORR) although it must be acknowledged that degradation of the ionomer and membrane may also contribute to the total performance loss particularly at higher temperatures such as 80 °C. Nevertheless, it would be useful to derive a theoretical relationship between the loss in EPSA and increase in the overpotential associated with the ORR and compare it to the experimentally observed behavior. If successful, this analysis will also give some insight into the extent of the contribution of electrode kinetics to the overall performance loss during the accelerated stress tests at different temperatures and provide an *in-situ* real-time and non-destructive diagnostic measure of performance degradation.

The derivation of the relation is made based on the assumptions that ORR kinetics obeys Tafel behavior and that the kinetic parameters (exchange current density and transfer coefficient) do not change over the course of an accelerated stress test. It also makes use of the fact that the EPSA and cell voltage are always measured at the same temperature (60 °C) regardless of the temperature during the application of the potential cycles. The derivation is presented in detail in Appendix and yields the following expression relating the change in EPSA to the change in the overpotential for ORR kinetics:

$$\frac{\Delta\eta_{\mathrm{kin}}}{E_{\mathrm{BOL}}} = b\frac{\log\left(\frac{\mathrm{EPSA}(N)}{\mathrm{EPSA}(0)}\right)}{E_{\mathrm{BOL}}} = b\frac{\log\left(1-\frac{\Delta\mathrm{EPSA}(N)}{\mathrm{EPSA}(0)}\right)}{E_{\mathrm{BOL}}} \tag{10}$$

where $\Delta\mathrm{EPSA} = \mathrm{EPSA}(0) - \mathrm{EPSA}(N)$, $\Delta\eta_{\mathrm{kinetic}} = \eta_{\mathrm{ORR},0} - \eta_{\mathrm{ORR},N}$ and EPSA(0) and EPSA(N) are the effective platinum surface areas in the BOL state and after N cycles, respectively. $\eta_{\mathrm{ORR},0}$ and $\eta_{\mathrm{ORR},N}$ are the activation overpotentials for the ORR in the BOL state and after N cycles, respectively, at a specified current density (0.1 A cm^{-2} in this case), b is the Tafel slope and E_{BOL} is the BOL cell voltage. Both sides of Equation (10) are divided by E_{BOL} to correct for sample-to-sample differences of the membrane electrode assemblies.

The following procedure is used to compare the predictions of Equation (10) to the observed behavior from measurements of the EPSA and the cell voltage at 0.1 A cm^{-2} of the MEAs in their BOL state and after 1000, 5000, 10,000 and 20,000 cycles of the accelerated stress tests conducted at 40, 60 and 80 °C. The experimental value of $\eta_{\mathrm{ORR},N}$ is obtained by subtracting the open-circuit voltage from the IR-corrected potential $E_{\mathrm{corr},N}$ obtained from the polarization curve at 0.1 A cm^{-2} after N cycles, i.e.,

$$\eta_{\mathrm{ORR},N} = E_{\mathrm{corr},N} - \mathrm{OCV} \tag{11}$$

The IR-correction is done by making use of R_s obtained from electrochemical impedance spectroscopy. Once $\eta_{\mathrm{ORR},N}$ is determined, it is then used to give $\Delta\eta_{\mathrm{kinetic}}$ and $\Delta\eta_{\mathrm{kinetic}}/E_{\mathrm{BOL}}$. The corresponding ΔEPSA is determined from the measured EPSA(0) and EPSA(N). A plot of $\Delta\eta_{\mathrm{kinetic}}/E_{\mathrm{BOL}}$ versus ΔEPSA/EPSA(0) then yields the experimental curves shown in Fig. 7 for the MEAs subjected to the accelerated stress tests at 40, 60 and 80 °C. The model-predicted curve is obtained from Equation (10) by substituting the measured E_{BOL} and arbitrary values of EPSA(N)/EPSA(0) into the right-hand side to compute $\Delta\eta_{\mathrm{kinetic}}/E_{\mathrm{BOL}}$ and then plotting this result versus ΔEPSA/EPSA(0). The value of b on the right-hand side of Equation (10) is evaluated using standard methods from a Tafel plot of the experimental polarization data. The relation computed according to Equation (10) appears as the solid curve in Fig. 7.

Examination of Fig. 7 indicates that Equation (10) correctly predicts the observed behavior in two important respects for ΔEPSA/EPSA(0) values up to approximately 20%. Firstly, the computed values of $\Delta\eta_{\mathrm{kinetic}}/E_{\mathrm{BOL}}$ agree well with the measured values over this range. Secondly, the experimental curves are found to be largely independent of the temperature during the accelerated stress tests at these lower ΔEPSA/EPSA(0) values. Such behavior is in fact expected based on Equation (10). Given that the EPSA and the cell performance are always characterized at the same temperature and that the kinetic parameters are assumed not to be altered by the potential cycling, Equation (10) predicts that the relation between $\Delta\eta_{\mathrm{kinetic}}/E_{\mathrm{BOL}}$ and ΔEPSA/EPSA(0) follows a single universal curve independent of the temperature. As ΔEPSA/EPSA(0)

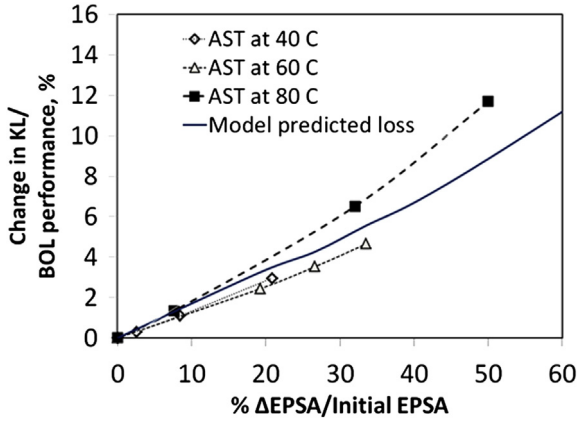

Fig. 7. Degradation – performance indicator obtained at 0.1 A cm^{-2} of a cell after being subjected to Pt dissolution ASTs at 40, 60 and 80 °C. Solid line corresponds to theoretical predictions using Equation (4).

increases above 20%, this expression is still able to describe the behavior of the MEA tested at 60 °C reasonably well over the entire duration of the accelerated stress test. On the other hand, the measured values of $\Delta\eta_{kinetic}/E_{BOL}$ in the MEA subjected to potential cycles at 80 °C begin to deviate more significantly from those obtained in the MEAs tested at the lower temperatures and are less accurately predicted by Equation (10). Taken together, these trends indicate that the kinetic losses at low current densities are associated mainly with the losses in EPSA during accelerated stress tests at 40 and 60 °C. However, when accelerated stress tests are conducted at 80 °C, other factors come into play, particularly during the later stages of the potential cycling when significant degradation of the catalyst has already occurred. This is consistent with the observation in Fig. 7 that the theoretical expression underestimates the loss in the actual measured cell voltage. At 80 °C, the degradation of other MEA components (e.g., ionomer and membrane) may become significant and/or the ionomer resistance may increase at the catalyst/membrane interface due to dehydration or humidity variations within the cathode layer [27]. Also, the exchange current density and Tafel slope, which are assumed to remain constant over the course of the accelerated stress test in the derivation of Equation (10) may actually change with time.

4. Conclusions

An accelerated stress testing protocol involving the application of potentiostatic square-waves with 3 s at 0.6 V followed by 3 s at 1.0 V was used to study Pt dissolution in MEAs at 40, 60 and 80 °C. Analysis of polarization curves during the course of the accelerated stress tests revealed degradation in MEA performance particularly at low current densities where kinetic effects are dominant. This was consistent with findings from other experimental techniques. The polarization resistance in the low current region measured using electrochemical impedance spectroscopy was found to increase upon aging at all three temperatures. Characterization of the ECSA using cyclic voltammetry revealed significant losses of catalyst at all temperatures particularly during the first 1000 square-wave cycles. In addition, these measurements showed that an increase in temperature led to higher losses of ECSA and electrocatalytic activity. On the other hand, very little change in the ohmic resistance was observed after the MEA was subjected to accelerated stress tests at 40 and 60 °C. Some increase in cell resistance was observed at 80 °C perhaps due to some degradation of the membrane and ionomer. This conclusion is supported by the polarization curve at 80 °C which showed some degradation in cell voltage at intermediate currents where ohmic effects become important.

A diagnostic signature expression relating the change in EPSA to the change in the activation overpotential of the oxygen reduction reaction in the low current region was developed and found to predict the observed behavior of the MEAs subjected to the potential cycling at 40 and 60 °C very well throughout the accelerated stress test. On the other hand, the diagnostic expression showed good agreement with the measured performance loss of the MEA at 80 °C only up to EPSA losses of 20% or less. These trends support the conclusion that degradation primarily involved the loss of Pt in the MEA at 40 °C and 60 °C, whereas both catalyst and membrane losses occurred at 80 °C. SEM images confirmed the formation of Pt bands in the membrane at all temperatures. More intense bands with larger Pt aggregates appeared in the images of the MEAs degraded at 60 and 80 °C, while a much thinner band was observed at 40 °C.

Acknowledgments

The authors gratefully acknowledge the Natural Sciences and Engineering Research Council of Canada (NSERC) and AFCC Corporation for funding this research. Appreciation is extended to the failure analysis team at AFCC for training one of the co-authors (SRD) to use SEM.

Appendix. Derivation of relation between ORR overpotential and EPSA

The contributions of the overpotential associated with the hydrogen oxidation reaction (HOR) are small under fully humidified conditions. Thus, the iR-corrected cell voltage E_{corr} for a PEMFC in the absence of oxygen diffusion losses can be written as [25,28]:

$$E_{corr} = E_{cell} + iR_s = E_{rev} - \eta_{ORR} \tag{A1}$$

where E_{cell} is the observed cell voltage (V), E_{rev} is the reversible cell potential (V), i is the applied current density (A cm^{-2}), R_s is the sum of the membrane, contact and bulk electronic resistances (ohm-cm^2) and η_{ORR} is the activation overpotential (V) of the ORR.

Assuming simple Tafel kinetics i.e., a single Tafel slope during the entire cathode potential range, the overpotential and current density for the ORR are related as follows [25]:

$$\eta_{ORR} = \frac{2.303RT}{n\alpha_c F}\log\left[\frac{i+i_x}{10U_{pt}L_w ECSA\, i_{o,s}\left(\frac{p_{O_2}}{p^*_{O_2}}\right)\exp\left[\left(\frac{E_c}{R}\right)\left(1-\frac{T}{T^*}\right)\right]}\right] \tag{A2}$$

where i is the measured cell current density (A cm^{-2}), i_x is the current density associated with H_2 crossover (A cm^{-2}), i_o is the catalyst specific exchange current density normalized to the reference oxygen partial pressure (A cm$^{-2}_{Pt}$), U_{Pt} is the catalyst utilization (%), ECSA is the electrochemical surface area (cm$^2_{Pt}$ mg$^{-1}_{Pt}$), L_w is the cathode loading of the MEA (g$_{Pt}$ m^{-2}), E_c is the activation energy (kJ mol^{-1}), F is the Faraday constant (96485 C mol^{-1}), R is the gas constant (8.314 J mol^{-1} K^{-1}), n is the number of electrons being transferred, α_c is the cathodic transfer coefficient, $p^*_{O_2}$ is the reference partial pressure of 101.3 kPa for O_2, p_{O_2} is the partial pressure of O_2 (kPa) under the fuel cell operating conditions. γ is the kinetic reaction order for the ORR, while T and T^* are the operating and reference temperatures (K). Pt utilization U_{Pt} of the MEA is assumed to be 0.8 [26], while γ is taken to be 0.75 based on the literature [28].

The EPSA can be related to the ECSA using Equation (A3):

$$EPSA = 10\, L_W\, U_{Pt}\, ECSA \tag{A3}$$

and substituted into Equation (A2) to yield:

$$\eta_{ORR} = \frac{2.303RT}{n\alpha_c F}\log\left[\frac{i+i_x}{EPSA\, i_{o,s}\left(\frac{p_{O_2}}{p^*_{O_2}}\right)^{\gamma}\exp\left[\left(\frac{E_c}{R}\right)\left(1-\frac{T}{T^*}\right)\right]}\right] \tag{A4}$$

Since the ORR is considered to obey Tafel kinetics, the applied current density i is large enough that $i >> i_x$. Thus, for the purposes of this analysis, Equation (A4) can be further simplified to:

$$\eta_{ORR} = b\log\left[\frac{i}{EPSA\, i_{o,s}\left(\frac{p_{O_2}}{p^*_{O_2}}\right)^{\gamma}\exp\left[\left(\frac{E_c}{R}\right)\left(1-\frac{T}{T^*}\right)\right]}\right] \tag{A5}$$

where $b = 2.303RT/n\alpha_c F$. During the *in-situ* experiments to obtain the polarization curves and EIS spectra, temperature and partial

pressure of O_2 are kept constant. Thus, the denominator EPSA $i_{o,s}(p_{O_2}/p^*_{O_2})^{\gamma} exp[(E_c/R)(1-T/T^*)]$ in Equation (A5) can be written as EPSA $i_{o,s}|_{T,P_{O_2}}$ where $i_{o,s}|_{T,P_{O_2}}$ is the exchange current density corresponding to the operating temperature and pressure. For convenience, this is written as i_o. Equation (A5) then becomes:

$$\eta_{ORR} = b \log\left[\frac{i}{\text{EPSA}\, i_o}\right] \tag{A6}$$

During the life testing of the PEMFC catalyst, the Tafel slope b and the exchange current density i_o are assumed to remain constant. Using the EPSA values measured after 0, 1000, 10,000 and 20,000 cycles, the overpotential η_{ORR} associated with the kinetics of the ORR can be calculated at a given i using Equation (A6) once b and i_o are known without the need of the polarization curve data. Thus, the overpotentials $\eta_{ORR,0}$ at the BOL state and $\eta_{ORR,N}$ after N accelerated stress test cycles, respectively, obtained at a given current density i can be expressed as:

$$\eta_{ORR,0} = b \log\left[\frac{i}{\text{EPSA}(0) i_o}\right] \tag{A7}$$

$$\eta_{ORR,N} = b \log\left[\frac{i}{\text{EPSA}(N)\, i_o}\right] \tag{A8}$$

where EPSA(0) and EPSA(N) are the effective platinum surface areas measured in the BOL state and after N accelerated stress test cycles. In order to account for the variations in the initial state of each MEA, the overpotential data for each MEA are expressed as the difference $\Delta\eta$ relative to the BOL overpotential for that MEA. Thus, $\Delta\eta$ is obtained by subtracting Equation (A8) from Equation (A7) to yield

$$\begin{aligned}\Delta\eta_{kin} &= \eta_{ORR,0} - \eta_{ORR,N} = b \log\left[\frac{\text{EPSA}(N)}{\text{EPSA}(0)}\right] \\ &= b \log\left(1 - \frac{\Delta\text{EPSA}(N)}{\text{EPSA}(0)}\right)\end{aligned} \tag{A9}$$

where ΔEPSA (N) = EPSA (0) − EPSA (N).

Finally, both sides Equation (A9) are normalized with respect to the BOL cell voltage E_{BOL} of the particular MEA to yield:

$$\frac{\Delta\eta_{kin}}{E_{BOL}} = b\frac{\log\left(1 - \frac{\Delta\text{EPSA}(N)}{\text{EPSA}(0)}\right)}{E_{BOL}} \tag{A10}$$

This normalization step is included to correct for the typical sample-to-sample variations in E_{BOL}.

All EPSA values obtained during the Pt dissolution accelerated stress tests are used in Equation (A10) in order to compute the theoretical polarization curve similar to that presented previously [29].

References

[1] C. He, S. Desai, G. Brown, S. Bollepalli, Electrochem. Soc. Interface 14 (2005) 41–44.
[2] P.J. Ferreira, G.J. la O', Y. Shao-Horn, D. Morgan, R. Makharia, S. Kocha, H.A. Gasteiger, J. Electrochem. Soc. 152 (2005) A2256–A2271.
[3] F.A. de Bruijn, V.A.T. Dam, G.J.M. Janssen, Fuel Cells 8 (2008) 3–22.
[4] R.L. Borup, J.R. Davey, F.H. Garzon, D.L. Wood, M.A. Inbody, J. Power Sources 163 (2006) 76–81.
[5] M.K. Debe, A.K. Schmoeckel, G.D. Vernstrom, R. Atanasoski, J. Power Sources 161 (2006) 1002–1011.
[6] W. Bi, T.F. Fuller, J. Electrochem. Soc. 155 (2008) B215–B221.
[7] W. Bi, G.E. Gray, T.F. Fuller, Electrochemical Solid-State Lett. 10 (2007) B101–B104.
[8] K. Yasuda, A. Taniguchi, T. Akita, T. Ioroi, Z. Siroma, Phys. Chem. Chem. Phys. 8 (2006) 746–752.
[9] M. Uchimura, S.S. Kocha, ECS Trans. 11 (2007) 1215–1226.
[10] M. Uchimura, S. Sugawara, Y. Suzuki, J. Zhang, S.S. Kocha, ECS Trans. 16 (2008) 225–234.
[11] S. Zhang, X.-Z. Yuan, J.N.C. Hin, H. Wang, K.A. Friedrich, M. Schulze, J. Power Sources 194 (2009) 588–600.
[12] J. Aragane, T. Murahashi, T. Odaka, J. Electrochem. Soc. 135 (1988) 844–850.
[13] S.C. Zignani, E. Antolini, E.R. Gonzalez, J. Power Sources 182 (2008) 83–90.
[14] J. Xie, D.L. Wood, K.L. More, P. Atanassov, R.L. Borup, J. Electrochem. Soc. 152 (2005) A1011–A1020.
[15] R.M. Darling, J.P. Meyers, J. Electrochem. Soc. 150 (2003) A1523–A1527.
[16] E. Hillstrom, Design and Validation of a Subscale PEMFC Test Hardware, in: Hydrogen + Fuel Cells International Conference 2011 Vancouver Canada (2011).
[17] S. Zhang, X. Yuan, H. Wang, W. Mérida, H. Zhu, J. Shen, S. Wu, J. Zhang, Int. J. Hydrogen Energy 34 (2009) 388–404.
[18] S.B. Brummer, J.I. Ford, M.J. Turner, J. Phys. Chem. 69 (1965) 3424–3433.
[19] X. Cheng, Z. Shi, N. Glass, L. Zhang, J. Zhang, D. Song, Z.S. Liu, H. Wang, J. Shen, J. Power Sources 165 (2007) 739–756.
[20] M. Inaba, T. Kinumoto, M. Kiriake, R. Umebayashi, A. Tasaka, Z. Ogumi, Electrochim. Acta 51 (2006) 5746–5753.
[21] P. Yu, M. Pemberton, P. Plasse, J. Power Sources 144 (2005) 11–20.
[22] X. Yuan, H. Wang, J. Colin Sun, J. Zhang, Int. J. Hydrogen Energy 32 (2007) 4365–4380.
[23] V. Atrazhev, S.F. Burlatsky, N. Cipollini, D. Condit, N. Erikhman, ECS Trans. (2006) 239–246.
[24] J. Zhang, B.A. Litteer, W. Gu, H. Liu, H.A. Gasteiger, J. Electrochem. Soc. 154 (2007) B1006–B1011.
[25] H. Gasteiger, W. Gu, R. Makharia, M. Mathias, B. Sompalli, Beginning of Life MEA Performance—efficiency Loss Contributions, Wiley Online Library, 2003.
[26] H.A. Gasteiger, S.S. Kocha, B. Sompalli, F.T. Wagner, Appl. Catal. B Environ. 56 (2005) 9–35.
[27] J. Zhang, Z. Xie, J. Zhang, Y. Tang, C. Song, T. Navessin, Z. Shi, D. Song, H. Wang, D.P. Wilkinson, Z.-S. Liu, S. Holdcroft, J. Power Sources 160 (2006) 872–891.
[28] K. Neyerlin, W. Gu, J. Jorne, H.A. Gasteiger, J. Electrochem. Soc. 153 (2006) A1955–A1963.
[29] J. Stumper, R. Rahmani, F. Fuss, ECS Trans. 25 (1) (2009) 1605–1615.